Attitude Determination using Infrared Earth Horizon Sensors

Tam Nguyen
Department of Aeronautics and Astronautics, Massachusetts Institute of Technology
77 Massachusetts Avenue, Cambridge, MA 02139; 617-710-1845
tamz@mit.edu

Faculty Advisor: Kerri Cahoy
Department of Aeronautics and Astronautics, Massachusetts Institute of Technology

ABSTRACT

Infrared Earth horizon sensors (EHS) are capable of providing attitude knowledge for satellites in low-Earth orbit, even during periods of eclipse. Attitude information is acquired by detecting Earth's infrared electromagnetic radiation and, subsequently, determining the region obscured by Earth in the sensors' fields of view to compute a nadir vector estimation in the satellite's body frame. Due to the limited computational resources and source code modification ability of most small satellites on orbit, a compact and robust EHS solution is required to efficiently achieve high-accuracy attitude knowledge. This paper presents the analytic form and simulated model of an attitude estimation method to compute a nadir vector using inputs from infrared EHS with Gaussian response characteristics. The proposed method can be applied when two sensors, each with known and distinct pointing directions, detect the horizon, which is defined as having their fields of view partially obscured by Earth. The accuracy of the estimation was quantified through simulations to be approximately 0.2° for a satellite in low-Earth orbit under a maximum attitude disturbance level of 4°. The sensitivity of the estimation accuracy relative to mounting uncertainty was also analyzed, yielding an additional error of 0.7° on nadir vector estimation for every 0.25° of boresight offset.

BACKGROUND

Robust attitude determination and control systems are often required for satellites on orbit to counter disturbances in nominal operation and to achieve mission-specific requirements. Attitude knowledge of small satellites is often achieved by devices such as sun sensors and magnetometers. However, these sensors have clear limitations: sun sensors lose their functionalities in periods of eclipse in orbit, while magnetometers cannot acquire high accuracy attitude measurements due to the constantly changing Earth magnetic field. Earth horizon sensors have emerged as efficient and relatively inexpensive means of more precise attitude determination, capable of satisfying attitude knowledge requirements of small satellites in low-Earth orbit (LEO), especially for missions with Earth-specific science objectives[1].

While the Sun and stars are effectively point sources from the perspective of a satellite in LEO, the Earth appears as a large and bright target that is easily detected. For a satellite in LEO at 500 km altitude, the Earth subtends a solid angle of 3.9 sr, significantly wider than the solid angle of the Sun (7×10^{-5} sr) and of Betelgeuse (6×10^{-14} sr). Due to the large expanse of the Earth in the spacecraft-centered unit sphere, detection of the horizon is required for precise satellite attitude knowledge. Horizon sensors provide the primary mean to directly determine the satellite's attitude with respect to the Earth[1].

Infrared Earth horizon sensors detect the Earth's electromagnetic radiation in the infrared spectrum, caused by the Sun's radiation being absorbed and re-radiated by the Earth's surface and atmosphere. In the long-wave infrared spectrum beyond 4 μm, the Earth becomes a dominant infrared radiation source, exceeding the Sun irradiation level by several orders of magnitude[2]. Infrared radiation is often referred to as thermal radiation due to the thermal energy generated by the emission of electromagnetic radiation in this spectrum. The

thermal energy emitted by Earth can be measured using thermopile detectors, devices that convert thermal energy collected in the sensor's field of view (FOV) into electrical energy. Commercial thermopile sensor units generally have Gaussian sensitivity, with the half-width at half-maximum (HWHM) defined as the effective half-angle field of view.

While large spacecraft often have EHS on scanning wheels[1], it is more practical for small satellites to have fix, body-mounted EHS system due to mass, volume, and power limitations. Thermopiles can be mounted on satellites at various locations with fixed and predetermined directions, depending on the mission altitude and sensors' FOV. Arrays of thermopiles have been utilized by small satellites to maintain nadir-pointing by ensuring zero temperature difference between sensors in each sensor pair along the velocity vector and side directions[4]. To fully determine the satellite's attitude in an inertial frame through the triad method, a full expression of the nadir vector in the satellite's body frame is needed. The second reference vector used in the triad method can be the Sun vector, acquired by sun sensors during day time, or the magnetic field direction, which can be determined using magnetometers during periods of eclipse.

This paper presents a method to compute a nadir vector estimation from two horizon sensor readings, corresponding simulation results and the estimation accuracy's sensitivity to mounting uncertainty. This estimation method is applicable when two sensors with distinct mounting boresight directions detect the horizon, corresponding to the case where the sensors' FOV are partially obscured by Earth. Depending on the sensors' FOV, EHS systems can be used for fine or coarse attitude knowledge.

The satellite's body coordinate system used in this paper is define as follows: the +x direction is along the nominal velocity vector, the +z direction nominally points toward nadir, and the +y direction points to the side of the spacecraft, completing a right-hand coordinate system. The two EHS are mounted along the x and y axes to provide pitch and roll knowledge of the satellite. In addition, each sensor are mounted with a dip angle in the z direction such that the horizon can be detected. This dip angle θ_z between the sensors' boresights and the x-y plane can be computed from the satellite's altitude (h), and the average Earth radius ($\overline{R_E}$), as shown in Equation 1. The EHS configuration used in this paper is shown in Figure 1, along with the satellite's coordinate system.

$$\theta_z = \cos^{-1}\left(\frac{\overline{R_E}}{\overline{R_E}+h}\right) \quad (1)$$

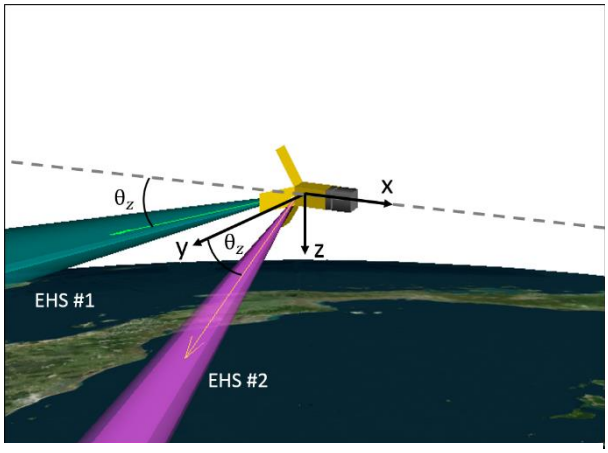

Figure 1 EHS mounting configuration in the satellite's body frame

This compact attitude estimation was developed to accommodate the limitations of small satellites memory and computation capabilities. To reduce the complexity needed for the method, the attitude estimation solution using EHS readings throughout this paper relies on the following assumptions: the Earth infrared emission at the wavelength of interest is uniform within the sensor's FOV, and the horizon curve observed by the sensor is circular.

ANALYTICAL NADIR VECTOR SOLUTION

This section presents a baseline model of the Earth and sensor geometry, leading to a preliminary estimation of the nadir vector. The analysis will start with the assumption that the sensor sensitivity is constant within the sensor's FOV. The sensor reading can therefore be assumed to be proportional to the area obstructed by Earth in the sensor's FOV. In addition, the angle subtended by Earth (the Earth disk radius) in the satellite's frame is modeled as a constant, which is only a good approximation when the satellite's altitude is unchanging. These two parameters, the sensor responsivity and the Earth disk radius, will be refined in the next section to

further improve the accuracy of the attitude estimation.

The area obstructed by Earth in the sensor's FOV, which directly correlates to the sensor reading, is modeled as the overlap area between the projections of the sensor's FOV and the Earth onto the spacecraft-centered unit sphere. Both projections are modeled as perfect circles with known angular radii. The center of the sensor field projection on the spacecraft-centered sphere represents the direction of the sensor boresight; and the center of the Earth disk denotes the direction of the nadir vector. A graphical representation of the geometry is shown in Figure 2.

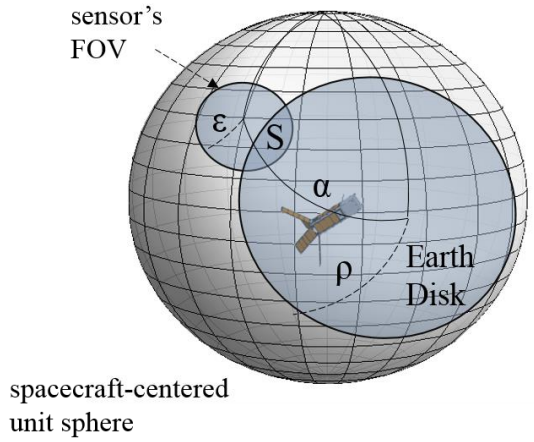

Figure 2 Projections of the sensor's FOV and the Earth on the spacecraft-centered unit sphere[1]

The overlap area S between the projections of the sensor's FOV of radius ε and the Earth disk of radius ρ represents the region obstructed by Earth within the sensor's FOV. The angle between the nadir vector and the sensor boresight is denoted by α. When $\alpha \geq \rho + \varepsilon$, the two circular projections do not overlap, representing the case where Earth is not detected by the sensor. On the other hand, when $\alpha \leq \rho - \varepsilon$, the sensor's FOV is fully obstructed by Earth, assuming the sensor's FOV is narrower than the Earth disk. The Earth's horizon is detected by the sensor when α is within the range $(\rho - \varepsilon, \rho + \varepsilon)$. The overlap area S in this range can be computed as a function of α, ε, and ρ as shown in Equation 2[1]. For known values of ε and ρ, this relationship allows the sensor reading, which can be directly correlated to S, to be converted to a nadir angle relative to a fixed and known vector in the spacecraft body frame, leading to partial attitude knowledge. Since it is computationally intensive to invert this equation to solve for α as a function of S, creating a look-up table is more practical for software implementation of this method.

$$
\begin{aligned}
&S(\alpha, \varepsilon, \rho) \\
&= 2\left[\pi - \cos(\rho)\cos^{-1}\left(\frac{\cos(\varepsilon) - \cos(\rho)\cos(\alpha)}{\sin(\rho)\sin(\alpha)}\right)\right. \\
&- \cos(\varepsilon)\ \cos^{-1}\left(\frac{\cos(\rho) - \cos(\varepsilon)\cos(\alpha)}{\sin(\varepsilon)\sin(\alpha)}\right) \\
&\left. - \cos^{-1}\left(\frac{\cos(\alpha) - \cos(\varepsilon)\cos(\rho)}{\sin(\varepsilon)\sin(\rho)}\right)\right]
\end{aligned}
\tag{2}
$$

To narrow down the set of solutions, at least two nadir angles relative to distinct boresight vectors are needed to provide a finite set of nadir vector solutions. The problem becomes finding the intersection of two cones, each with a different axis direction, defined by the sensor boresight vector, and a cone angle, which is the nadir angle computed in the previous step. The geometric solutions can be visualized using Figure 3. $\widehat{S_1}$ and $\widehat{S_2}$ represent the sensor boresights; φ_1 and φ_2 are the corresponding nadir angles; $\hat{P}$ and $\hat{P}'$ are the intersections of the S_1-centered and S_2-centered cones, representing the two possible nadir vectors.

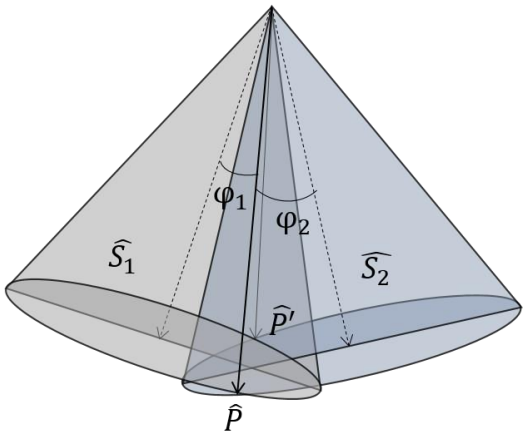

Figure 3 Graphical representation of the possible nadir vectors, given two nadir angles relative to two reference vectors.

The analytical form of the possible nadir vectors are the solutions to the system of equations 3. The first two equations ensure that the angles between the solutions and the boresight vectors equal to the nadir angles found in the previous steps. The third equation is a normalization condition, which is required for the first two equations to hold. This

system of three equations consists of exactly three variables, which are the three components of the nadir vector. It can be solved analytically through variable eliminations and substitutions for a finite set of solutions. Algebraically, there can be zero, one, or two vector solutions to the system of equations since the third equation is of second order. When both sensors detect the horizon, the system of equations has at least one solution, assuming low sensor noise level. The system of equations has exactly one solution when the satellite is oriented such that the nadir vector is on the plane containing $\widehat{S_1}$ and $\widehat{S_2}$, which is unlikely to occur due to jitters and other disturbances. In most cases, there are two possible nadir vector solutions to the system of equations, leading to ambiguity in the estimation results.

$$\begin{cases} \hat{\mathrm{P}} \cdot \widehat{S_1} = \cos(\varphi_1) \\ \hat{\mathrm{P}} \cdot \widehat{S_2} = \cos(\varphi_2) \\ \left|\hat{\mathrm{P}}\right| = 1 \end{cases} \qquad (3)$$

The physical interpretation of this ambiguity can be visualized in the scenarios presented in Figure 4. The attitude in the bottom subfigure is the result of rotating the satellite, which is initially in the attitude in the top subfigure, about the boresight of one sensor until the other sensor detects the other side of the Earth's horizon. The two scenarios yield the same EHS readings since both sensors are obstructed by Earth by the same amount. However, in the scenario in the bottom subfigure, the z-axis is no longer in alignment with the nadir vector as in the scenario in the top subfigure.

The ambiguity can be resolved by the use of an additional coarse sensor, given that the two possible nadir vector solutions ($\hat{P}$ and $\hat{P}'$) are well separated. It can be seen in the geometrical representation (Figure 3) as well as proven algebraically that $\hat{P}$ and $\hat{P}'$ are reflections of each other through the plane containing vectors $\widehat{S_1}$ and $\widehat{S_2}$. Therefore, the angle separation between $\hat{P}$ and $\hat{P}'$ is twice the angle between $\hat{P}$ and the $\widehat{S_1}$-$\widehat{S_2}$ plane, as illustrated in Figure 5. The angle separation between $\hat{P}$ and $\hat{P}'$, denoted as $\theta_{PP'}$, can be computed as shown in Equation 4.

$$\theta_{PP'} = 2\left|\sin^{-1}\left(\hat{P} \cdot \frac{(\widehat{S_1} \times \widehat{S_2})}{|\widehat{S_1} \times \widehat{S_2}|}\right)\right| \qquad (4)$$

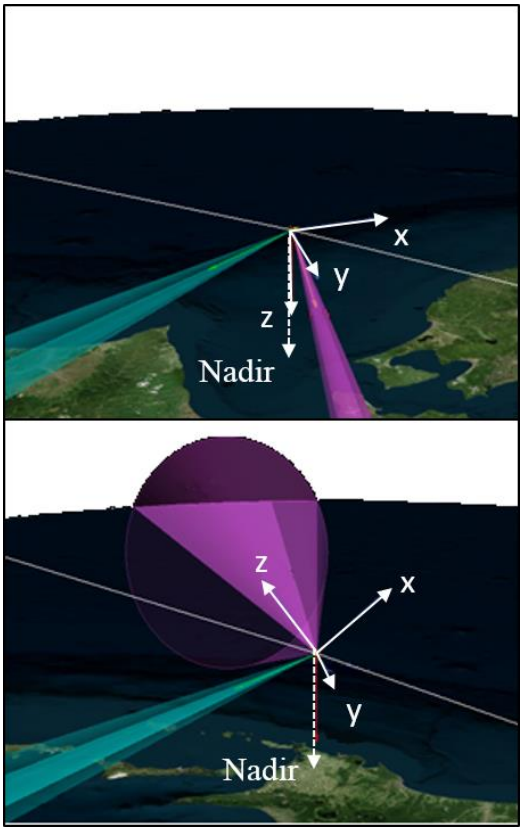

Figure 4 Ambiguity in attitude determination using EHS readings. The scenario in the second subfigure yield the same sensor readings as in the first subfigure while the satellite's z-axis is no longer in alignment with the nadir vector.

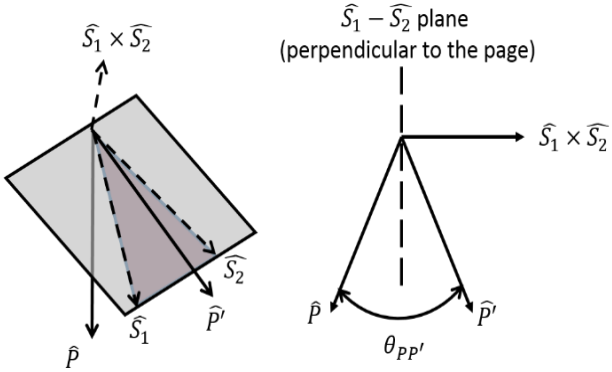

Figure 5 Geometric illustration of the angle separation between the two possible nadir vectors

The separation angle between the possible nadir solutions depends on the relative position of the nadir vector ($\hat{P}$) and the sensor boresight vectors ($\widehat{S_1}$ and $\widehat{S_2}$). When the sensors have narrow FOV, the

sensor readings are only valid when one of the possible nadir solutions is in near alignment with the z-axis. In this case, the separation angle can be reduced to the expression in Equation 5 below, where θ_z was introduced in Equation 1.

$$\theta_{PP'} \cong 2 \left| \sin^{-1}\left(\frac{\cos\theta_z}{\sqrt{1+\sin^2\theta_z}}\right) \right| \quad (5)$$

At an altitude of 500 km and with sensors' FOV half-angle of 5°, the angle separation between the two possible nadir solutions $\theta_{PP'}$ is approximately 120° when one of the solutions aligns with the z-axis and 106° in the worst case scenario. Because of this wide separation angle, the ambiguity can be easily resolved during nadir acquisition by comparing the two possible solutions to the reading of an additional coarse attitude sensor, such as sun sensors or magnetometers. While wide FOV sensors increases the range of attitude in which EHS are valid, the separation angle between the nadir solutions could be significantly reduced. For example, when the FOV half-angle is 30°, the separation angle can be as narrow as 2.3° in the worst case scenario. This ambiguity requires an additional coarse sensor with better resolution to be resolved. In practice, it is advantageous to use an EHS system with wide FOV and/or other coarse sensors to acquire close to nadir-pointing such that another EHS system with narrow FOV can be used to determine more accurate attitude knowledge.

MODEL REFINEMENTS

Gaussian sensitivity

The analysis in the previous section assumes that the sensor sensitivity is constant within the sensor's FOV. Most commercial thermopiles, however, have Gaussian responsivity characteristics[3]. This section will describe how the Gaussian pattern of the sensor sensitivity can be incorporated into the model to improve the accuracy of the nadir vector estimation.

Since modeling the sensor sensitivity as a continuous 2D Gaussian function significantly increases the complexity of the obscuration calculation, the sensor field can instead be divided into regions of constant sensitivity to approximate the Gaussian pattern. Figure 6 shows an example of such Gaussian approximation with three constant sensitivity regions, where the darker color indicates higher sensitivity. The overlap area of the Earth disk and each sensor regions are denoted as S_1, S_2, S_3. By using the overlap function $S(\alpha, \varepsilon, \rho)$ from Equation 2, the overlap areas S_1, S_2, S_3 can be computed by changing the sensor's angular radius parameter ε to the corresponding FOV half-angle of each sensor region. These calculations are shown in Equations 6, where r_1, r_2, r_3 ($r_1 < r_2 < r_3$) denote the radii of the regions' circular boundaries as projected onto a unit sphere around the satellite.

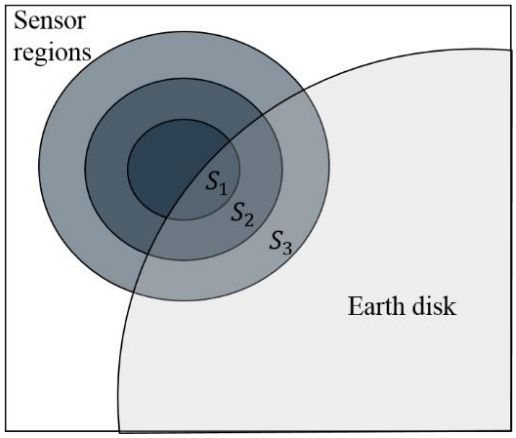

Figure 6 Obscuration model with sensor field divided into regions of constant sensitivity

$$\begin{cases} S_1 = S(\alpha, r_1, \rho) \\ S_2 = S(\alpha, r_2, \rho) - S(\alpha, r_1, \rho) \\ S_3 = S(\alpha, r_3, \rho) - S(\alpha, r_2, \rho) \end{cases} \quad (6)$$

The sensor response becomes the weighted sum of S_1, S_2, S_3 with the appropriate Gaussian approximation coefficients. The sensor response values can be pre-computed for different values of nadir angles to construct a look-up table. This look-up table, consisting of the modified sensor response and the corresponding nadir angle, can be saved in flight software for efficient nadir angle conversion for on-orbit operation.

Altitude correction

The half-angle subtended by Earth from the satellite's reference frame, denoted by ρ, was assumed to be constant in the previous analyses. However, this assumption results in significant inaccuracy in attitude estimation in the case of satellites in high-eccentricity orbit or in de-orbiting phase. Since most satellites have position knowledge through the Global Positioning System

(GPS) or Two-line Element (TLE) data, this information can be used to better estimate the angle subtended by Earth in the satellite's frame ρ, improving the accuracy of the estimation method.

It can be observed that ρ is a function of the orbit radius and the Earth radius at the horizon. For satellites with low altitude, this Earth radius can be approximated as the Earth radius directly under the satellite. The Earth's half-angle ρ can be approximated as shown in Equation 7, where $\vec{r}$ represents the satellite's position vector in an Earth-centered reference frame. The orbit radius $R(\vec{r})$ is computed as the magnitude of the position vector. The Earth radius directly under the satellite $R'_E(\vec{r})$ can be computed using the World Geodetic System 84 Ellipsoid Earth model. Note that to avoid additional complexity, the Earth shape is still assumed to be spherical with radius $R'_E(\vec{r})$ in other parts of the analysis. As a result, the angle subtended by Earth from the satellite reference frame can be estimated efficiently in real time based on the satellite's position knowledge. The satellite's orbit radius and Earth radius configuration is illustrated in Figure 7.

$$\rho \cong \sin^{-1}\left(\frac{R'_E(\vec{r})}{R(\vec{r})}\right) \cong \sin^{-1}\frac{\left(\frac{\cos^2(\theta_{gc}(\vec{r}))}{a^2}+\frac{\sin^2\left(\theta_{gc}(\vec{r})\right)}{b^2}\right)^{-1/2}}{|\vec{r}|} \quad (7)$$

where
$\theta_{gc}(\vec{r})$: geocentric latitude of satellite
a: Earth's equatorial radius
b: Earth's polar radius

SIMULATION MODEL

To verify the accuracy of the attitude estimation method presented above, a Satellite Tool Kit (STK) model was created for a small satellite in LEO, deployed from the International Space Station (ISS) and propagated using the STK built-in High-Precision Orbit Propagator (HPOP) tool. The orbit profile used in this analysis is presented in Figure 8. The altitude varies from 400 km to 430 km within one orbit.

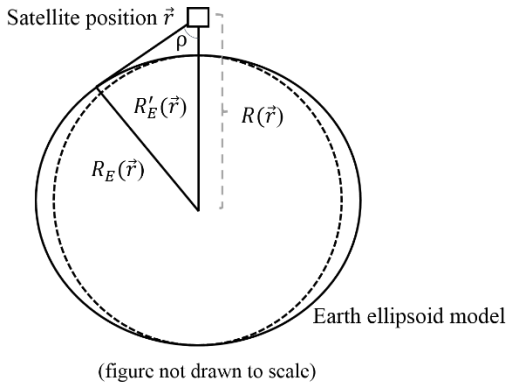

Figure 7 Satellite's position and Earth shape geometry. The half angle subtended by Earth from the satellite reference frame can be estimated from the satellite's position.

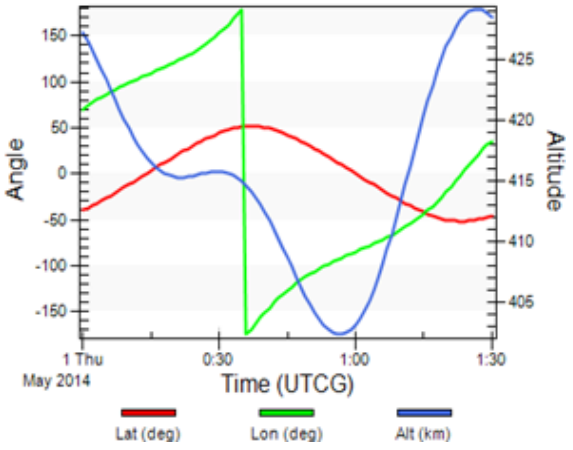

Figure 8 Simulated orbit profile of a small satellite in LEO, deployed from the ISS.

The satellite carries 6 thermopile sensors: 3 are mounted in the –x direction and 3 on the +y direction. All sensors have Gaussian sensitivity with FOV half-angle of 5°. The 3 sensors on each mount are reserved to be looking at deep space, Earth horizon, and Earth, and are tilted in the +z direction by 10°, 20°, and 30°, respectively. The sensor looking at deep space is not obstructed by Earth and is used as a "cold" reference for the horizon sensor reading. Similarly, the sensor designated to look at Earth provides a "hot" reference for the horizon sensors. The obscuration percentage of the horizon sensor can be computed using these two references to mitigate the effect of varying infrared emission from Earth's surface and background disturbances.

The satellite is modeled to spin around the z-axis, which initially aligns with the nadir vector. Attitude disturbances are manually introduced by setting a fixed nutation level for the spinning motion. For the following analysis, the nutation level was set to be 4°. At this level of disturbance, the EHS system is capable of providing a nadir vector at all times during the orbit. A graphical representation of the attitude setting is shown in Figure 9.

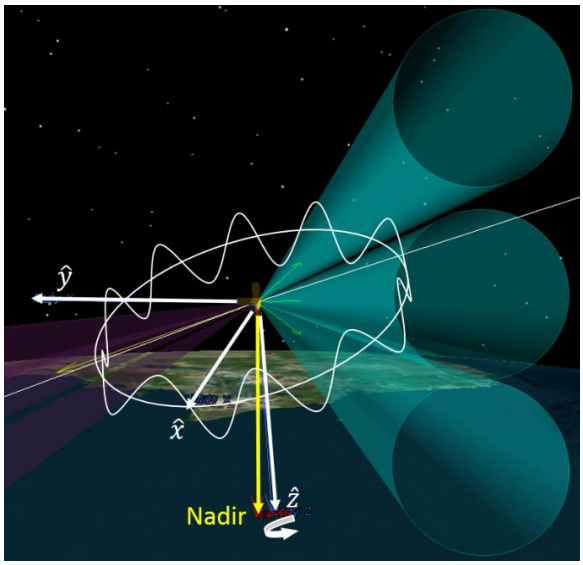

Figure 9 Simulated attitude profile. The satellite rotates about nadir direction with a maximum disturbance level of 4°.

SIMULATION RESULTS

The estimated nadir vector can be compared with the nadir vector extracted directly from the STK model, which is considered to be the "truth" reference in this analysis. The STK obscuration tool was used to find the percentage of the sensor field obstructed by Earth. Given two horizon sensors, the attitude estimation method previously presented was used to compute a unique estimate of the nadir vector. Ambiguity is resolved by assuming that the satellite's z-axis is near nadir pointing.

The angle between this estimated vector and the true nadir vector yields a quantitative measure of the accuracy of the estimation. Figure 10 shows the angular separation between the estimated nadir vector and the true nadir vector in the data set. The average accuracy of the estimation is 0.18° with a 1-σ variation of 0.082°. This error is mainly caused by modeling the Earth as a sphere in the obscuration model. Figure 11 shows the errors in x, y, z directions of the estimated nadir unit vector when being compared to the true nadir unit vector over the duration of one orbit. It can be observed that the z-component of the estimated nadir vector achieves higher accuracy than the x and y components by an order of magnitude.

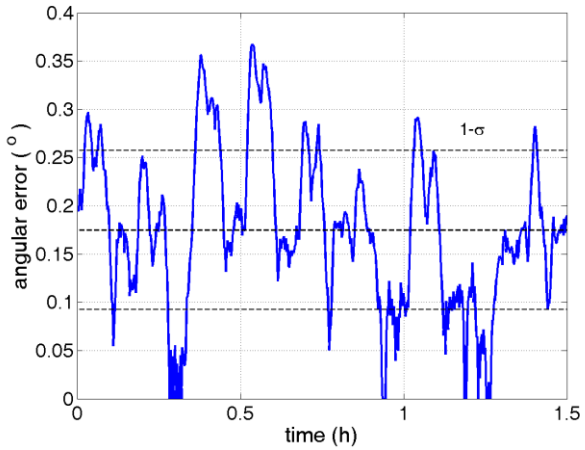

Figure 10 Angular error of the nadir estimation in simulation. The average angular error is (0.18 +/- 0.082)°.

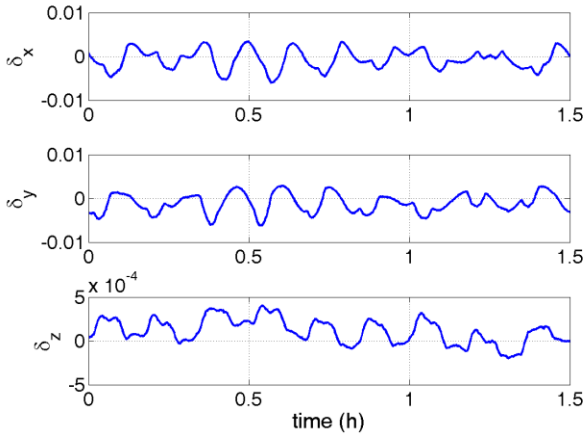

Figure 11 Nadir vector error in x, y, and z directions.

Without Gaussian sensitivity consideration and real-time altitude correction, the accuracy of the estimation is significantly reduced. When the sensor is modeled as having Gaussian characteristics, using the uniform sensitivity approximation in the estimation process leads to an additional error of approximately 0.95°. If the satellite altitude is not corrected using position knowledge but assumed to be constant at an average

value throughout the orbit, the altitude estimation error is increased by 0.1°. This error increase is expected to be higher for satellites in high-eccentricity orbits and in de-orbiting phase.

SENSITIVITY TO MOUNTING ERRORS

The nadir estimation accuracy results presented above rely on the perfect knowledge of sensor boresight directions, which were used as body-fixed reference vectors. Since the sensor boresight directions do not align with the satellite's body axes but tilted in the z-direction to allow horizon sensing, mounting errors are likely to occur during the assembly process of the sensor unit, mostly in the z-tilt angle θ_z. Different levels of boresight direction offset were input to the model. The attitude estimation accuracy for each boresight direction offset case and the corresponding best fit line is presented in Figure 12.

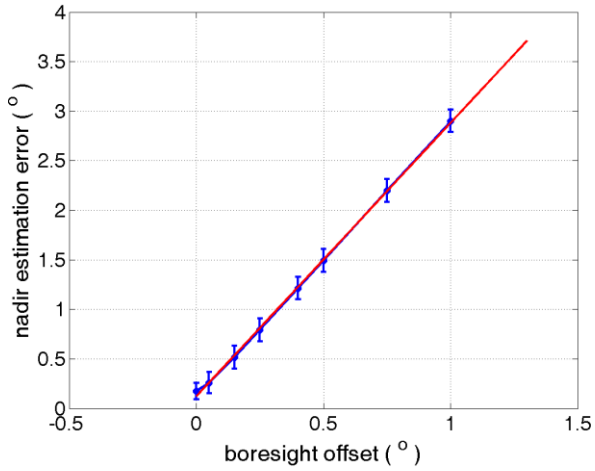

Figure 12 Attitude error as a function of sensors' mounting offset

The relationship between the boresight direction error and nadir estimation error follows a linear correlation, with a slope of 2.8°. This result implies that an error of 0.25° on each sensor boresight direction can lead to an additional error of 0.7° in the nadir estimation. Due to this high level of sensitivity, the sensors' boresight directions must be measured with high precision and accuracy to ensure accurate attitude estimates.

CONCLUSION AND FUTURE WORK

This paper presents a method to provide satellites' attitude knowledge by using two fixed body-mounted Earth horizon sensors. A nadir vector was computed in the satellite's body frame through modeling the Earth's obscuration in the sensor's FOV. The model was further refined to account for the sensor's non-uniform sensitivity and for the Earth disk size in the satellite's frame as a function of position in orbit. The accuracy of the estimation method was verified through simulation to be 0.18° on average with a 1-σ variation of 0.082°, assuming the sensors' responses and mounting directions are known with high precision. The estimation error increases linearly with sensors' boresight mounting error by a constant factor of 2.8°. If the boresight of each sensor can only be measured with 0.25° precision, the maximum total error of the estimation method is expected to be 0.88°.

To further analyze the accuracy of the estimation method, the sensor response scaling and biasing errors as well as random disturbances will be modeled in simulation. In addition, the attitude estimation method presented was implemented in the attitude determination and control of MIT's 3U CubeSat Micro-sized Microwave Atmospheric Satellite (MicroMAS), which is scheduled to be launched in June 2014. The telemetry data from MicroMAS will be analyzed to evaluate the performance of the Earth horizon sensors and the attitude estimation method on orbit.

ACKNOWLEDGEMENTS

The author would like to thank Professor Kerri Cahoy for her guidance throughout the project, fellow graduate students Meghan Prinkey, Anne Marinan, and the rest of the MIT MicroMAS team for their valuable support and feedback.

REFERENCES

[1] Wertz, J. (1978). *Spacecraft attitude determination and control*. Dordrecht, Holland: D. Reidel Publishing Company.

[2] Merrelli, A. (2012). *The Atmospheric Information Content of Earth's Far Infrared Spectrum*. (Doctoral dissertation).

[3] Thermopile Detector - TPD 1T 0214 G9 / 3850. Sensor Solutions. Product Specification. Revision 01/24/2013.

[4] Janson, S. et al. (2012) *Attitude Control on the Pico Satellite Solar Cell Testbed-2*. The Aerospace Corporation. 26th Annual AIAA/USU Conference on Small Satellites.